Morphology Parameters for Intracranial Aneurysm Rupture Risk Assessment

Sujan Dhar, B.E.,
Department of Mechanical and Aerospace Engineering, State University of New York, University at Buffalo, Buffalo, New York

Toshiba Stroke Research Center, Buffalo, New York

Markus Tremmel, Ph.D.,
Departments of Neurosurgery and Radiology, State University of New York, University at Buffalo, and Millard Fillmore Gates Hospital, Kaleida Health, Buffalo, New York

Toshiba Stroke Research Center, Buffalo, New York

J Mocco, M.D., M.S.,
Departments of Neurosurgery and Radiology, State University of New York, University at Buffalo, and Millard Fillmore Gates Hospital, Kaleida Health, Buffalo, New York

Toshiba Stroke Research Center, Buffalo, New York

Minsuok Kim, Ph.D.,
Department of Mechanical and Aerospace Engineering, State University of New York, University at Buffalo, Buffalo, New York

Toshiba Stroke Research Center, Buffalo, New York

Junichi Yamamoto, M.D., Ph.D.,
Departments of Neurosurgery and Radiology, State University of New York, University at Buffalo, and Millard Fillmore Gates Hospital, Kaleida Health, Buffalo, New York

Toshiba Stroke Research Center, Buffalo, New York

Adnan H. Siddiqui, M.D., Ph.D.,
Departments of Neurosurgery and Radiology, State University of New York, University at Buffalo, and Millard Fillmore Gates Hospital, Kaleida Health, Buffalo, New York

Toshiba Stroke Research Center, Buffalo, New York

L. Nelson Hopkins, M.D., and
Departments of Neurosurgery and Radiology, State University of New York, University at Buffalo, and Millard Fillmore Gates Hospital, Kaleida Health, Buffalo, New York

Toshiba Stroke Research Center, Buffalo, New York

Hui Meng, Ph.D.
Departments of Mechanical and Aerospace Engineering, Neurosurgery, and Radiology, State University of New York, University at Buffalo, and Millard Fillmore Gates Hospital, Kaleida Health, Buffalo, New York

Toshiba Stroke Research Center, Buffalo, New York

Abstract

OBJECTIVE—The aim of this study is to identify image-based morphological parameters that correlate with human intracranial aneurysm (IA) rupture.

METHODS—For 45 patients with terminal or sidewall saccular IAs (25 unruptured, 20 ruptured), three-dimensional geometries were evaluated for a range of morphological parameters. In addition to five previously studied parameters (aspect ratio, aneurysm size, ellipticity index, nonsphericity index, and undulation index), we defined three novel parameters incorporating the parent vessel geometry (vessel angle, aneurysm [inclination] angle, and [aneurysm-to-vessel] size ratio) and explored their correlation with aneurysm rupture. Parameters were analyzed with a two-tailed independent Student's *t* test for significance; significant parameters ($P < 0.05$) were further examined by multivariate logistic regression analysis. Additionally, receiver operating characteristic analyses were performed on each parameter.

RESULTS—Statistically significant differences were found between mean values in ruptured and unruptured groups for size ratio, undulation index, nonsphericity index, ellipticity index, aneurysm angle, and aspect ratio. Logistic regression analysis further revealed that size ratio (odds ratio, 1.41; 95% confidence interval, 1.03−1.92) and undulation index (odds ratio, 1.51; 95% confidence interval, 1.08−2.11) had the strongest independent correlation with ruptured IA. From the receiver operating characteristic analysis, size ratio and aneurysm angle had the highest area under the curve values of 0.83 and 0.85, respectively.

CONCLUSION—Size ratio and aneurysm angle are promising new morphological metrics for IA rupture risk assessment. Because these parameters account for vessel geometry, they may bridge the gap between morphological studies and more qualitative location-based studies.

Keywords

Intracranial aneurysm; Morphology; Rupture risk; Size ratio; Vessel geometry

---

Intracranial aneurysms (IA) affect approximately 2 to 5% of the entire population (23,25). Ruptured IAs typically cause subarachnoid hemorrhage (SAH) and its sequelae, resulting in significant morbidity and mortality. Among patients who have SAH, 50 to 60% will die from the initial hemorrhage and a further 20 to 25% will experience complications (30). However, despite their expected common occurrence, only 1% of all IAs actually rupture (25). Although the morbidity and mortality associated with rupture may suggest that an incidentally detected aneurysm should be treated to forestall the catastrophic event of SAH, the two current methods of treatment (open microsurgical aneurysm clip ligation or endovascular aneurysm coil embolization) are not without some risk of major morbidity and mortality (8,31). Therefore, an accurate metric (or several metrics) to judge the risk of rupture of an aneurysm is critical to aid in generating the best possible treatment algorithm.

Hemodynamics has been shown to play an important role in IA pathophysiology and rupture. Using computational fluid dynamics, Hassan et al. (11) suggested that high wall shear stress (WSS) may be responsible for IA growth and rupture in high-flow aneurysms, whereas the predominant factors causing rupture in low-flow aneurysms are high intra-aneurysmal pressure and flow stasis. Cebral et al. (6) demonstrated that ruptured IAs have unstable flow patterns,

smaller impinging jet diameters, and smaller impingement zones. Shojima et al. (24) found that ruptured IAs have a higher average WSS in the aneurysm sac than unruptured IAs. They observed recirculation zones and blood stasis at the apex of ruptured IAs.

It is important to realize that IA hemodynamics are strongly dependent on the geometry of the aneurysmal sac and its feeding vessel (11,13,26). For a given geometry, Cebral et al. (5) showed that hemodynamics do not vary significantly with physiological variations of flow rate, blood pressure, and waveform. Therefore, suitable parameters characterizing IA geometry can capture the characteristic hemodynamics and potentially predict rupture risk. Several past studies have investigated such parameters.

The most ubiquitous parameter is IA size. Although aneurysms exceeding 10 mm in size are considered to be dangerous, several studies have shown that a large percentage of ruptured aneurysms are, in fact, smaller than 10 mm (2,9,22,23,26,27,30). The relationship between IA rupture risk and IA size has yet to be completely elucidated.

Aneurysm shape has been studied as well, and certain shape parameters show stronger correlation with rupture than IA size. Aspect ratio (AR), defined as IA height divided by neck diameter, is the most commonly studied shape parameter. Although most findings affirm its importance, they do not converge on a common threshold value (2,22,26,27,29). Other, more sophisticated, shape parameters such as undulation index (UI), nonsphericity index (NSI), and ellipticity index (EI) have been proposed (22) in an attempt to account for the three-dimensional (3D) nature of IA. Such 3D parameters show promise to be better predictors than lower-dimensional parameters such as size or AR, and they are further examined in the current study.

Previous studies have also investigated additional factors that correlate with IA rupture risk, such as familial preponderance, smoking, hypertension, female sex, connective tissue disorder, aneurysm growth rate, and presence of multiple IAs (15-17,32). However, these studies have not yielded quantifiable metrics that can be readily integrated into the clinical decision-making process. Adding complexity from such diverse variables into our current study would make risk assessment analysis unwieldy. Currently, morphometric evaluation, typically using size alone, is the mainstay of applied aneurysm rupture risk assessment in day-to-day clinical practice. Our aim is to improve such morphological evaluation and better the accuracy of aneurysm rupture risk assessment, something that is fundamental to the current practice of cerebrovascular neurosurgery.

A limitation of previous morphology-based rupture risk studies, including those investigating 3D parameters, is that the geometry of the parent artery is typically ignored. Parent artery geometry has a significant influence on the resultant IA hemodynamics and, consequently, the rupture risk. Castro et al. (4) have demonstrated that upstream vessel tortuosity can critically influence intra-aneurysmal hemodynamics. Hassan et al. (11) observed that a greater parent vessel incidence angle shifts the high WSS area toward the aneurysm dome, where rupture-prone blebs often are present, whereas Hoi et al. (13) noted that highly curved parent vessels subject IAs to higher hemodynamic stresses at the inflow zone that might promote growth or rupture. Thus, parent vessel geometry should be accounted for when defining morphological parameters for IA rupture risk prediction. Furthermore, numerous studies have observed a connection between IA rupture risk and vessel location (3,4,9,21,26,30). Because vessel location is strongly related to vessel geometry, this finding affirms the importance of vessel geometry for IA rupture risk. Incorporating parent vessel geometry in morphology parameters can, at least to some extent, capture the influence of IA location as well.

In the current study, we address the above-mentioned issues and define three new morphology parameters that incorporate IA parent vessel geometry. We analyze a group of 45 IAs (20

ruptured, 25 unruptured) to evaluate new IA rupture parameters, in comparison with five "traditional" parameters that have been described in earlier studies.

PATIENTS AND METHODS

Study Population and Tools Used

During a 2-year period (2006−2007), 3D rotational digital subtraction angiography images were collected for patients with saccular terminal or sidewall intracranial IAs treated at Millard Fillmore Gates Hospital. All images collected were examined for suitability to be included in the study. Because 3D data reconstructed from rotational angiographic images (as opposed to two-dimensional [2D] images) were used in this study, we could only include cases in which the rotational angiographic images were of sufficient quality for accurate segmentation and reconstruction. Forty-five consecutive patients with 25 unruptured and 20 ruptured aneurysms met these criteria. Sixteen aneurysms (11 unruptured, 5 ruptured) were classified as saccular sidewall lesions, and 29 aneurysms (14 unruptured, 15 ruptured) were classified as saccular terminal lesions by the treating neurosurgeons. The aneurysm location and the age and sex of the patients were known. Approval for the collection and review of data was obtained from the Institutional Review Board at the University at Buffalo.

The 3D angiography images were obtained with a Toshiba Infinix VFi/BP frontal C-arm system (frame rate, 25 frames/s; rotation rate, 50 degrees/s; field of view: 9 inches; Toshiba America Medical Systems, Inc., Tustin, CA), yielding an image stack of 512^3 pixels with a resolution of 0.19 to 0.25 mm/pixel. 3D reconstruction in surface-triangulation format and isolation of the region of interest (IA plus adjacent vessels) were performed using in-house software based on the open-source Visualization Tool Kit libraries. To allow accurate geometry measurements of both the aneurysm and the parent vessel, they were computationally separated at the IA neck using cutting tools in ANSYS ICEM CFD software (ANSYS, Inc., Canonsburg, PA). The IA neck plane was defined to our best ability as the location from where the aneurysmal sac pouched outward from the parent vessel. The 3D IA and parent vessel geometries were then analyzed to provide the various morphology parameters using custom algorithms programmed in MATLAB R2007a (MathWorks, Inc., Natick, MA). Finally, statistical analysis of the obtained data was performed using standard software tools (Microsoft Excel 2003, MATLAB R2007a, SPSS 15.0).

Definition of Parameters

Eight morphology parameters were investigated, five of which have been described previously. Additionally, we defined three new parameters, each of which incorporated the geometry of the parent vessel. A description of all eight parameters follows.

Size—Aneurysm size was defined, in accordance with Raghavan et al. (22), as the maximum perpendicular height of the IA; i.e., the maximum perpendicular distance of the dome from the neck plane (Fig. 1A).

Aspect Ratio—The aneurysm AR was defined as the ratio of the maximum perpendicular height to the average neck diameter, where the average neck diameter was calculated as twice the average distance from the neck centroid to the edge of the neck (Fig. 1A) (26,27).

Undulation Index—The aneurysm UI was defined as $UI = 1 − (V/V_{ch})$, where V is the volume of the aneurysm above the neck plane and V_{ch} is the volume of the convex hull (22). The convex hull of the IA is the smallest volume that fully encloses the IA volume and that is convex at all points. It resembles a plastic wrap attached to the neck and stretched over the IA surface (Fig. 1B). The parameter UI captures the degree of IA surface concavity, which can be

significant when the aneurysmal sac has strong undulations or when daughter aneurysms are present. The UI increases with the number and severity of concave regions on the IA surface. Conversely, a shape that is nonconcave (e.g., a perfect sphere or a cube) will have a UI of 0.

Ellipticity Index—The EI characterizes the deviation of the IA convex hull from that of a perfect hemisphere, and is thus a measure of IA elongation. It is defined as $EI = 1 - (18\pi)^{1/3} V_{ch2/3}/S_{ch}$, where S_{ch} is the surface area of the convex hull (22). Based on the convex hull, the EI is independent of undulations. In contrast to AR, which uses one-dimensional lengths, the EI characterizes IA elongation based on 3D variables such as volume and surface area.

Nonsphericity Index—The NSI is similar to the EI, but it uses the actual aneurysm volume and surface area to characterize the deviation of the IA geometry from that of a perfect hemisphere. It is defined as $NSI = 1 - (18\pi)^{1/3} V^{2/3}/S$, where S is the IA surface area (22). This parameter is influenced by ellipticity and surface undulations and hence can be thought of as a combination of EI and UI.

In addition to the traditional parameters listed above, we defined three new parameters as follows:

Size Ratio—The aneurysm-to-vessel size ratio (SR) incorporates the geometries of the IA and its parent vessel and was defined as $SR = $ (maximum aneurysm height)/(average vessel diameter). Here, the average vessel diameter (D_V) was obtained by measuring two representative vessel cross sections upstream of the aneurysm (D_1 at the proximal neck and D_2 at $1.5 \times D_1$ upstream), calculating the local diameters in the same way as the neck diameter, and taking their average value. The maximum height in the above equation is not the maximum perpendicular height (H) used in the calculation of size and AR. Rather, it is the maximum (not necessarily perpendicular) distance from the centroid of the aneurysm neck to any point on the aneurysm dome (H_{max}). Thus, SR captures the maximum deformation to the parent vessel caused by the outpouching of an IA. The maximum height of the aneurysm and the locations in the vessel used to define SR are shown in Figure 2. In the case of a terminal aneurysm, the IA bulges out from several vessels. Therefore, the average diameter of the feeding and all branching vessels was used for the "average vessel diameter" in this case.

Vessel Angle—Apart from the aneurysm geometry, the parent vessel inlet angle relative to the aneurysm has been shown to have a large effect on intraaneurysmal flow (11,13,28). The vessel inlet angle or simply, the vessel angle (θ_V), was defined as the angle between the inlet vessel centerline and the neck plane (Fig. 2). The centerline is approximated by the line connecting the centroids of the two vessel cross sections used to define "average vessel diameter" in SR. It should be noted that θ_V is only defined for sidewall IAs. Because the value of θ_V depends on the direction from which the geometry is viewed, a rigorous definition of the viewing plane is necessary and will be given at the end of this section.

Aneurysm Inclination Angle—Because IA hemodynamics will also be influenced by the angle at which the IA is tilted with respect to the incoming flow, we defined the aneurysm inclination angle (θ_A) as another morphological metric. This is the angle of inclination between the IA and its neck plane (Fig. 2). The line inside the IA used for defining θ_A is the connection of the neck centroid to the farthest point on the IA dome. Aneurysms with daughter aneurysms and secondary growth are expected to have a higher value of this angle. As with θ_V, the θ_A is only defined for sidewall IAs and depends on the direction from which the geometry is viewed. The definition of the viewing plane is given below.

The viewing plane used for the definition of θ_V and θ_A was chosen so that it captures the direction of the incoming flow entering a side-wall IA. In other words, the velocity vectors of

the flow immediately upstream of the IA should lie inside the viewing plane. Most geometries in patients have vessels that bend in all three dimensions, and it is essential to view the geometry from a direction at which that incoming flow is visible. The correct viewing plane is determined as follows:

1. First, the geometry is rotated until the neck plane is seen as a line. That means that the IA neck plane must be perpendicular to the viewing plane.

2. Then, an axis of rotation through the neck centroid is defined perpendicularly to the neck plane, and the entire geometry is rotated about this axis. The view that results in the lowest value of the apparent vessel angle (apparent θ_V) is chosen to be the viewing plane in which θ_V and θ_A are finally measured.

Even though θ_A, at first glance, seems to have no relation with the parent vessel, it is important to note that θ_A is just as dependent on the viewing plane as θ_V. If the viewing plane was chosen differently, the measured θ_A would also be different.

The MATLAB codes for analyzing the above morphological parameters in this study are published in the public domain to enable verification of this work (12).

Statistical Analysis

The first six morphological parameters described above (size, AR, UI, EI, NSI, SR) were calculated for each IA, whereas the last two (θ_V and θ_A) were only calculated for sidewall IAs. The means and the standard deviations of each parameter were calculated separately for the ruptured and unruptured subgroups. Scatter plots for all parameters were produced, distinguishing between ruptured and unruptured IAs and showing the means for the ruptured and unruptured groups, respectively. A Jarque-Bera test for departure from a normal distribution was performed on each parameter. The null hypothesis that the parameters belonged to a normal distribution was not rejected at the level of 5% significance by the Jarque-Bera test at any instance. Data "outliers" were identified for each parameter from box-and-whisker plots. Then, a two-tailed independent Student's t test was performed for each parameter (excluding the outliers) to assess the statistical significance of the observed difference between the means of ruptured and unruptured groups. P values and 95% confidence intervals from the t test were calculated and reported.

The parameters found to be significant ($P < 0.05$) in the Student's t test were further analyzed using multivariate logistic regression (backward elimination) to identify those parameters that retained significance when accounting for all relevant variables. Logistic regression was performed on AR, UI, EI, NSI, and SR for all IAs, and in a second run on AR, UI, EI, NSI, SR, and θ_A for sidewall IAs only. Before performing the regression, each of the variables was scaled to span a range from 0 to 10, thereby ensuring that a unit increase in the parameter corresponds to 10% of its observed range. This makes the odds ratios obtained for the variables easily comparable. At each regression step, the analysis yields a model for the odds of rupture, which was reported with the odds ratios, the 95% confidence intervals, and the P values. The final equation for the odds of rupture contains only those parameters that are significant after the model has been adjusted for correlations between parameters.

Receiver operating characteristic (ROC) analysis was also performed for all parameters excluding the outliers (22,29). The ROC curves were plotted, and area under the curve (AUC) values for each parameter were calculated and compared. The ROC curves and the AUC indicate the limits of a parameter's ability to discriminate between the two subgroups—ruptured and unruptured aneurysms. Thresholds for optimal sensitivity and specificity were also calculated for parameters that were found to be significant.

RESULTS

To clearly present parameter values for all unruptured and ruptured cases, we plotted each variable (vertical axis) against AR (horizontal axis), which is the most well-known morphological index that has been shown to be associated with IA rupture risk. The 2D scatterplots for the traditional parameters and the new parameters are shown in Figures 3 and *4*, respectively. A visual inspection of the means for the unruptured (*solid circle*) and the ruptured (*solid square*) IAs shows a clear separation between ruptured and unruptured groups, except for size and θ_V. From Figure 3, we also observe an obvious correlation between AR and NSI, and between AR and EI, which is expected since NSI and EI both measure IA elongation, similar to AR. It may also be observed that UI has the least correlation with AR. The values for the means along with standard deviations are given in Table 1.

Box-and-whisker plots of each parameter for ruptured and unruptured IAs are shown in Figures 5 and 6. Such plots are a useful method to identify outliers. The *horizontal line* within the box is the median (or the 50th percentile), whereas the upper and lower bounds of the box represent the 75th and the 25th percentiles, respectively. The *whiskers* on either side represent the last data points that lie within 1.5 box heights from the 75th and 25th percentile points. Data points further outside (shown by "+") are regarded as outliers and have not been considered for the Student's *t* test and the ROC analysis. Size, NSI, SR, and θ_V plots (Figs. 5 and 6) show one outlier each. AR had the maximum number of outliers (n = 3); UI, EI, and θ_A had no outliers.

From the Student's *t* test, significant differences were found between ruptured and unruptured means for SR (2.8 ± 1.1 versus 1.8 ± 0.84, $P < 0.001$), UI (0.12 ± 0.070 versus 0.063 ± 0.045, $P < 0.001$), NSI (0.24 ± 0.06 versus 0.16 ± 0.076, $P < 0.01$), EI (0.19 ± 0.043 versus 0.14 ± 0.062, $P < 0.01$), and AR (1.5 ± 0.45 versus 1.2 ± 0.55, $P < 0.05$) (Table 1). Size and θ_V means were not significantly different (Table 1).

To identify optimal thresholds for IA rupture, ROC analysis (excluding the outliers) was performed for each of the parameters (33). Sensitivity and specificity values were calculated for a range of thresholds; the resulting curves are shown in Figure 7A. The *dashed line* along the middle of the plot is the null predictor. One way to quantify the ability of a parameter to discriminate between ruptured and unruptured groups is to calculate the AUC; i.e., the area under the ROC curve. The results are given in Table 1 and Figure 7B. θ_A and SR had the highest AUC values (0.85 and 0.83, respectively), whereas θ_V and size both showed small AUC values (0.54 and 0.58, respectively). Note that the null predictor had an AUC of 0.5. Optimal thresholds for all the parameters are also identified and tabulated.

Multivariate logistic regression analysis was performed on variables found to be significant in the *t* test to identify parameters that show significant correlation with ruptured IAs when controlling for correlations between variables. The regression was performed on AR, UI, EI, NSI, and SR for all IAs, and in a second run on AR, UI, EI, NSI, SR and θ_A for sidewall IAs only. Having regressed for the variables using a backward elimination process, the final parsimonious model for assessing aneurysm rupture risk (odds) was obtained:

$$\text{Odds} = e^{0.412 \times UI + 0.342 \times SR - 3.80} \tag{1}$$

We note that only UI and SR are left as independently signifi-cant parameters. The odds of rupture increase by a factor of 1.51 for a unit increase in UI, and by a factor of 1.41 for a unit increase in SR. For every step of the regression, the coefficients (β) of the model along with the odds ratios, 95% confidence intervals, and *P* values are listed in Table 2.

The second logistic regression analysis (only for sidewall IAs) also yielded SR and UI as the two remaining independently significant parameters (equation not shown). It did not yield

θ$_A$ as independently significant, even though θ$_A$ is a significant parameter with a high AUC value ($P < 0.05$ and AUC = 0.855). This is attributable to a strong correlation of θ$_A$ with AR.

DISCUSSION

In this study, we have tested five existing and three new parameters for correlation with IA rupture. Among the new parameters, SR and θ$_A$ achieved statistical significance ($P < 0.05$). Furthermore, a logistic regression analysis on all eight parameters showed that SR and UI are independently correlated with ruptured IAs.

Size Ratio and Relation to IA Location

SR was found to be an important and significant parameter for IA rupture risk ($P < 0.001$). Seventy-seven percent of all ruptured aneurysms had SRs greater than 2.05 (the optimal threshold distinguishing the ruptured from unruptured IAs), whereas 83% of all unruptured aneurysms had SRs of less than 2.05. SR takes into account not only the aneurysm size itself but also the local vessel caliber and incorporates it into a quantifiable parameter. By doing so, it indirectly accounts for the effect of IA location on rupture.

Several studies have related IA rupture risk to aneurysm location. A particularly high rupture risk exists in the anterior regions of the circle of Willis, and a large percentage of small aneurysms that rupture are located on the anterior communicating artery (AComA) (1,2,9,21, 22). One such study was conducted by Beck et al. (2), who analyzed 155 aneurysms and concluded that the majority of small (<7 mm) ruptured aneurysms occurred in the anterior circulation (69.4%). They also observed that aneurysms at the AComA were significantly more often ruptured than unruptured ($P = 0.02$). Orz et al. (21) reported that 30.1% of 1088 ruptured aneurysms were located on the AComA, and they concluded that the most common site of small aneurysm rupture is the AComA. In contrast to the high rupture incidence in the anterior circulation, it was also found that IAs on the cavernous part of the internal carotid artery (ICA) and on the ophthalmic artery seldom rupture (9,25,29,30).

Carter et al. (3) analyzed the reason for the trends observed in the above studies. They studied 854 ruptured and 819 unruptured aneurysms and found that the locations for ruptured lesions, when ordered by decreasing average aneurysm size, were ophthalmic artery, ICA bifurcation, basilar bifurcation, middle cerebral artery bifurcation, posterior communicating artery, AComA, posteroinferior cerebellar artery, and "distal" locations, where "distal" was defined as an IA located distally on A2, P2, or M2 bifurcations. IAs in such distal locations rarely grew to sizes larger than 10 mm. From a correlation with associated vessel sizes, they noted that average sizes of ruptured IAs are smaller on vessels of smaller sizes. To explain this trend, they conjectured that aneurysms arising from smaller vessels will have walls that are thinner and, according to Laplace's Law (10), experience much greater wall tension when they are subjected to the same pressures as IAs with greater wall thickness. Thus, they state that the relative resistance to rupture of two aneurysms of the same size but arising from vessels with different sizes and different wall thicknesses may be different. In general, vessel size and wall thickness decrease behind branching points, and the more distally an IA is located in the arterial tree, the smaller its wall thickness and parent vessel diameter will be.

From the above studies, it appears that the influence of IA location on rupture risk is at least partly related to the relationship between IA size and parent vessel diameter. However, the classification of aneurysms into categories solely on the basis of the "general" location (i.e., parent vessel name) is somewhat qualitative and cannot capture local variations in IA and vessel geometry. For example, the middle cerebral artery consists of several segments, each having a distinct geometry. Additionally, from individual to individual, the vessel diameters may vary significantly. To resolve this dilemma, we related aneurysm geometry to the local vessel

geometry via the SR. Instead of comparing the absolute sizes of aneurysms in different locations, the SR compares their sizes in a manner that accounts for the local parent artery diameter.

The fact that IAs rupture most often on the AComA and least on the ICA may be at least partly accounted for by the parameter SR. For example, a 5-mm aneurysm on the AComA (average diameter, 2 mm) has a large SR of 2.5 (high rupture risk), but the same size aneurysm on the ICA (average diameter, 4 mm) has an SR of only 1.25 (low rupture risk). Evaluating Equation 1 for these two SRs reveals that, in fact, the odds of rupture for the first aneurysm are about 10 times higher than for the second. Especially when the parent vessel has a varying diameter or when clear trends based on general IA location do not exist, the SR can detect differences in rupture risk where size or location alone cannot.

The question arises as to whether the vessel diameter itself— rather than the SR—influences the correlation with IA rupture. We tested this hypothesis and found that vessel diameter was indeed significant ($P < 0.05$) (Fig. 8A). However, all data points in Figure 8A with vessel diameters exceeding 3 mm correspond to sidewall IAs located on the ICA (cavernous ICA and ICA adjacent to the ophthalmic artery), which are known to have a very low rupture risk from location-based studies (21,27,29,30). We therefore excluded these low-risk locations and evaluated the vessel diameter significance for only the remaining locations (Fig. 8B). We found that, for the remaining locations, the vessel diameter was no longer significant ($P = 0.125$), whereas SR was still significant ($P = 0.0045$) (Fig. 8C). In other words, when cases with clear location-based trends are included, such as the very low-risk ICA versus other vasculature, the vessel diameter may appear to show a strong correlation, but this does not hold when such clear-cut cases are excluded. Thus, we can reiterate that SR has an impressive correlation with rupture risk.

Aneurysm Angle

The second new parameter found to be statistically signifi-cant for rupture and to have good predictability was aneurysm angle, which is defined for sidewall aneurysms only. Eighty percent of all ruptured sidewall IAs had aneurysm angles greater than 112 degrees (the optimal threshold distinguishing the two groups), whereas 81.8% of all unruptured sidewall IAs had aneurysm angles less than 112 degrees.

The association of larger aneurysm angles with higher rupture risk may be linked to the presence of daughter aneurysms (or blebs on the main aneurysm sac), which is known to be correlated with increased IA rupture risk (18). We found that such blebs are usually located on the dome side opposed to incoming flow, causing a higher aneurysm angle (Fig. 9). In addition, Jou et al. (14) found that the highest rates of IA growth typically occur in the regions of lowest WSS (located at the far end of the dome), whereas Chatziprodromou et al. (7) observed that the main direction of IA growth was aligned with the direction of the incoming flow. Thus, a greater θ_A with respect to the parent vessel could be caused either by the presence of a daughter aneurysm/bleb, or by increased growth of the IA in the direction of the flow.

Aspect Ratio, Undulation Index, Nonsphericity Index, and Ellipticity Index

These parameters are shape indices that have been proposed in previous studies. In the present work, we included them in our analysis to have a basis of comparison for assessing the correlative potential of our newly defined parameters SR, θ_A, and θ_V with IA rupture.

The AR has been studied widely and has consistently been found to correlate with IA rupture. Statistical analysis performed by Ujiie et al. (26,27) showed the AR to be significant regardless of IA location, whereas IA size was not. Complex flow patterns with slow secondary flow were

observed by Ujiie et al. in IAs with an AR greater than 1.6. In contrast to this finding, Beck et al. (2) reported the AR of unruptured IAs to be higher than the AR of ruptured IAs (mean, 2.3 versus 1.8). Weir et al. (29) performed an ROC analysis to show that AR had an AUC value of 0.79, whereas size had an AUC of only 0.62. Both AR and size were found to be statistically significant ($P < 0.01$) in the study conducted by Weir et al. (29). In a study of 27 IAs (9 ruptured and 18 unruptured), Raghavan et al. (22) also found the AR to be statistically significant, with an ROC-AUC value of 0.72. AR achieved statistical significance in the present study.

Researchers have struggled to agree upon an optimal AR threshold value above which IAs may be deemed as dangerous. The threshold value of AR obtained from the current study is 1.18, compared with 1.6 reported by Ujiie et al. (27). One reason for this difference may be that Ujiie et al. used 2D angio-graphic data, whereas the present study used 3D data reconstructed from rotational angiography.

The parameters NSI, EI, and UI, originally proposed by Raghavan et al. (22), were also evaluated here. In the present study, NSI, EI, and UI were all found to be significant for IA rupture.

Aneurysm Size and Vessel Angle

Aneurysm size has been studied extensively as a parameter for rupture risk prediction. Rinkel et al. (23) reviewed nine studies in which size was considered as a possible metric for aneurysm rupture risk and found that the annual risk of rupture for an aneurysm greater than 10 mm in size was 1.9%, although it was 0.7% for an aneurysm smaller than 10 mm. Beck et al. (1), on the other hand, reported that neither height nor width was a significant predictor of rupture. Forget et al. (9) studied 245 cases and found that 85.6% of ruptured IAs were smaller than 10 mm. In a study by Nahed et al. (20), it was found that 65.7% of ruptured aneurysms were smaller than 7 mm, whereas the median size of all ruptured aneurysms was 5 mm. However, the correlation between IA rupture and size was not significant ($P = 0.61$). Raghavan et al. (22) found aneurysm height to be a non-significant rupture predictor ($P = 0.175$). From the above studies, it is evident that the correlation between IA rupture risk and size is not always statistically significant. In the present work, aneurysm size did not achieve statistical significance and had a low AUC value, which is in agreement with the studies discussed above.

The vessel angle (θ_V) was the last new parameter we proposed with the goal of incorporating more of the parent vessel geometry into IA rupture risk assessment. θ_V did not achieve statistical significance in our study. This is because most of the IAs in our patient group had vessel angles close to 0 degrees, as can be seen from the box plots in Figure 6, and there was little variation between the ruptured and the unruptured groups.

Multiple Logistic Regression Analysis of the Significant Parameters

The Student's t test and the ROC analysis yielded results showing that SR, AR, UI, NSI, EI, and (for sidewall IA) θ_A had significant correlations ($P < 0.05$). However, it is possible that some of these parameters may, in fact, be surrogate markers for others. To find an equation for the odds of IA rupture that only includes independently significant markers, multiple logistic regression was performed. At the end of the regression, only SR and UI remained as the independent and significant parameters in the model (Table 2 and Equation 1). The odd ratios reported in Equation 1 have been adjusted for the magnitude of the parameters so that a unit change in the value of the parameters is equivalent to a change of 10% of its observed range (0.394 for SR, 0.024 for UI). For a 10% increase in SR of an IA, the odds of its rupture increase by 1.41 times; and for a 10% increase in UI of an IA, the odds of its rupture increase by 1.51 times. AR, NSI, and EI are eliminated in the regression analysis. This can be explained by the scatterplots in Figures 3 and 4 , where it is obvious that SR, NSI, and EI each have a strong

correlation with AR (and thus, with each other). Because SR shows the strongest correlation among these, only SR was left as an independent parameter after the logistic regression. UI, on the other hand, was also significant and does not have a strong correlation with AR (Fig. 3). Therefore, UI remained as a second independent parameter in the logistic regression analysis. It is important to note that the final model obtained (Equation 1) requires measurement of both SR and UI to evaluate the odds of IA rupture. Although SR can easily be estimated from an angiographic image, the calculation of UI requires a 3D computational reconstruction, which might be difficult to perform in clinical examinations on a daily basis. Therefore, a routine evaluation of IA rupture risk in a clinical setting would probably not rely on Equation 1, but on measurement of SR and its optimal threshold of 2.05, which separates the unruptured and ruptured groups.

Limitations of the Present Study

One concern about this study was that our ruptured aneurysm data could have been affected by vasospasm. It is well accepted that vasospasm affects the parent artery on which the hemorrhage occurs from approximately 5 days after the hemorrhage (19). However, the vast majority of our patients present for evaluation and have imaging via rotational angiography within 24 hours of the initial hemorrhage. Therefore, vaso-spasm is not expected to have a significant effect on our data. To further examine this, we compared the average diameters of the parent vessels from our group with typical vessel diameters reported in the literature and found them to be within the normal range for all cases (Table 3). Also, as discussed earlier, there was no clear trend of ruptured IA vessel diameters being smaller than unruptured IA vessel diameters after the very low-risk ICA cases were excluded (Fig. 8B), which suggests that our data were not affected by vasospasm.

Another concern was that our ruptured aneurysm data could have been affected by the rupture itself; i.e., the shape or size of the ruptured IA might have changed owing to the rupture. To our knowledge, no study has been conducted that looks at the change in IA shape or size owing to rupture, but some studies have indicated that the size and shape of an aneurysm are not affected much by rupture (2,22,27). The reason for the lack of such studies might be that an IA is rarely imaged both before and after SAH. However, we were able to locate one clinical case in which 2D images existed both pre- and post-SAH. This case was a 51-year-old woman diagnosed with a posterior communicating artery IA that was not treated upon detection. Four months after the initial diagnosis, the patient sustained SAH. At that point in time, the posterior communicating artery IA was again imaged and then treated. The 2D views from the angiogram are shown in Figure 10. It appears that the aneurysm shape experienced a change after SAH. However, both IA height and parent vessel diameter remained constant before and after rupture, giving a constant SR of 2.6 using either of the images. On the basis of the optimal SR threshold of 2.05 found in our study, this particular aneurysm could have been identified as prone to rupture and treated while still unruptured. Unfortunately, only 2D images were available for this case; thus, it was not possible to evaluate other parameters, such as UI and NSI, for differences between pre- and post-SAH. This case argues against the hypotheses of significant aneurysmal changes, particularly reduction, in size after hemorrhage.

We acknowledge that one of the main limiting factors of the present study is the comparatively small size of the patient population. However, we believe that the absence of 2D approximations in the current work will lead to parameter measurements with a high degree of accuracy, compensating to an extent for the small study population. In the future, further 3D studies with larger populations will be required to corroborate the findings from this study.

As with all retrospective studies, the data for the ruptured IAs may have been affected by the event of the rupture itself. If this is the case, retrospectively determined indices may not be useful for aneurysm rupture risk assessment. However, to the extent possible with the data, the

change of IA size or shape owing to rupture and the influence of vasospasm on the results have been addressed in the present work. From this limited evidence, rupture does not seem to significantly affect the geometry of an aneurysm. Our study, which analyzed the correlation potential of various morphological parameters with IA rupture, can be valuable for identifying targets for IA rupture risk predictors in future prospective studies.

We acknowledge that we have not studied other risk-related factors such as smoking, hypertension, age, sex, and familial predisposition. The focus of the current study was to isolate purely morphological metrics that may correlate with IA rupture. A more comprehensive multivariate analysis including the above parameters would provide additional insight.

Finally, we would like to mention that, although a study of morphological metrics can be extremely useful for clinicians to assess aneurysm rupture risk, it cannot serve to directly explain the complex biological processes that lead to IA rupture. In this article, we have pointed out the connection of SR to IA location and thickness of the local parent artery wall. However, it must be noted that the aneurysm wall itself is a dynamic structure that is subject to a multitude of biological processes. In addition to the initial wall thickness, which is roughly determined by parent vessel location, such processes will further influence or compromise the strength of the wall to resist rupture. Future studies should aim at identifying biological conditions that might be included as additional parameters, along with the morphology metrics, and analyze their significance to assess IA rupture risk.

CONCLUSION

We examined eight 3D geometry-based IA morphological indices for correlation with ruptured and unruptured IAs, including three that were defined here for the first time, to account for the relationship with parent vessel geometry and location. Of the three new parameters, SR and aneurysm angle were found to be significant by the Student's *t* test ($P < 0.05$), with optimal thresholds beyond which an IA may be deemed dangerous being 2.05 and 112 degrees, respectively. Of the traditional parameters, AR, UI, NSI, and EI were found to be significant, whereas aneurysm size did not achieve statistical significance. A multivariate logistic regression was performed on all significant parameters, yielding the following model for estimating odds of rupture: odds $= e^{0.412 \times UI + 0.342 \times SR - 3.80}$, which involves only two independent parameters. SR and UI showed independent and significant correlation with ruptured IAs. From the findings in the present retrospective study, we propose that parameters that simultaneously quantify aneurysm shape and adjacent vessel geometry, such as SR and θ_A, have greater promise for IA rupture risk assessment than parameters based on aneurysm shape or size alone. These parameters also have the advantage of being easily calculable from angiography images and, thus, may be of practical use to neurosurgeons in their treatment decision-making process. The parameters identified to be significant in this study may be further evaluated in clinical studies to provide greater understanding into their potential for IA rupture risk assessment.

Acknowledgments

ABBREVIATIONS

2D, two-dimensional

3D, three-dimensional
AComA, anterior communicating artery
AR, aspect ratio
AUC, area under curve
EI, ellipticity index
IA, intracranial aneurysm
ICA, internal carotid artery
NSI, nonsphericity index
ROC, receiver operating characteristic
SAH, subarachnoid hemorrhage
SR, size ratio
UI, undulation index
WSS, wall shear stress

REFERENCES

1. Beck J, Rohde S, Berkefeld J, Seifert V, Raabe A. Size and location of ruptured and unruptured intracranial aneurysms measured by 3-dimensional rotational angiography. Surg Neurol 2006;65:18–27. [PubMed: 16378842]

2. Beck J, Rohde S, el Beltagy M, Zimmermann M, Berkefeld J, Seifert V, Raabe A. Difference in configuration of ruptured and unruptured intracranial aneurysms determined by biplanar digital subtraction angiography. Acta Neurochir (Wien) 2003;145:861–865. [PubMed: 14577007]

3. Carter BS, Sheth S, Chang E, Sethl M, Ogilvy CS. Epidemiology of the size distribution of intracranial bifurcation aneurysms: Smaller size of distal aneurysms and increasing size of unruptured aneurysms with age. Neurosurgery 2006;58:217–223. [PubMed: 16462474]

4. Castro MA, Putman CM, Cebral JR. Computational fluid dynamics modeling of intracranial aneurysms: Effects of parent artery segmentation on intraaneurysmal hemodynamics. AJNR Am J Neuroradiol 2006;27:1703–1709. [PubMed: 16971618]

5. Cebral JR, Castro MA, Appanaboyina S, Putman CM, Millan D, Frangi AF. Efficient pipeline for image-based patient-specific analysis of cerebral aneurysm hemodynamics: Technique and sensitivity. IEEE Trans Med Imaging 2005;24:457–467. [PubMed: 15822804]

6. Cebral JR, Castro MA, Burgess JE, Pergolizzi RS, Sheridan MJ, Putman CM. Characterization of cerebral aneurysms for assessing risk of rupture by using patient-specific computational hemodynamics models. AJNR Am J Neuroradiol 2005;26:2550–2559. [PubMed: 16286400]

7. Chatziprodromou I, Tricoli A, Poulikakos D, Ventikos Y. Haemodynamics and wall remodelling of a growing cerebral aneurysm: A computational model. J Biomech 2007;40:412–426. [PubMed: 16527284]

8. de Tribolet N, Bijlenga P. Intracranial aneurysms: Is there still a place for neurosurgery? Acta Neurochir (Wien) 2006;148:121–126. [PubMed: 16416036]

9. Forget TR Jr, Benitez R, Veznedaroglu E, Sharan A, Mitchell W, Silva M, Rosenwasser RH. A review of size and location of ruptured intracranial aneurysms. Neurosurgery 2001;49:1322–1326. [PubMed: 11846931]

10. Hademenos GJ, Massoud T, Valentino DJ, Duckwiler G, Viñuela F. A nonlinear mathematical model for the development and rupture of intracranial saccular aneurysms. Neurol Res 1994;16:376–384. [PubMed: 7870277]

11. Hassan T, Timofeev EV, Saito T, Shimizu H, Ezura M, Matsumoto Y, Takayama K, Tominaga T, Takahashi A. A proposed parent vessel geometry-based categorization of saccular intracranial aneurysms: Computational flow dynamics analysis of the risk factors for lesion rupture. J Neurosurg 2005;103:662–680. [PubMed: 16266049]

12. Hemodynamics Laboratory, Department of Mechanical and Aerospace Engineering, State University of New York at Buffalo. CVM Research: Algorithms for morphology parameter calculations on intracranial aneurysms. [12/11/2007]. http://www.eng.buffalo.edu/Research/Hemo/morph.htm.

13. Hoi Y, Meng H, Woodward SH, Bendok BR, Hanel RA, Guterman LR, Hopkins LN. Effects of arterial geometry on aneurysm growth: Three-dimensional computational fluid dynamics study. J Neurosurg 2004;101:676–681. [PubMed: 15481725]

14. Jou LD, Wong G, Dispensa B, Lawton MT, Higashida RT, Young WL, Saloner D. Correlation between lumenal geometry changes and hemodynamics in fusiform intracranial aneurysms. AJNR Am J Neuroradiol 2005;26:2357–2363. [PubMed: 16219845]

15. Juvela S. Risk factors for multiple intracranial aneurysms. Stroke 2000;31:392–397. [PubMed: 10657411]

16. Juvela S, Hillbom M, Numminen H, Koskinen P. Cigarette smoking and alcohol consumption as risk factors for aneurysmal subarachnoid hemorrhage. Stroke 1993;24:639–646. [PubMed: 8488517]

17. Kamitani H, Masuzawa H, Kanazawa I, Kubo T. Bleeding risk in unruptured and residual cerebral aneurysms—Angiographic annual growth rate in nineteen patients. Acta Neurochir (Wien) 1999;141:153–159. [PubMed: 10189496]

18. Meng H, Feng Y, Woodward SH, Bendok BR, Hanel RA, Guterman LR, Hopkins LN. Mathematical model of the rupture mechanism of intracranial saccular aneurysms through daughter aneurysm formation and growth. Neurol Res 2005;27:459–465. [PubMed: 15978170]

19. Morgan M, Halcrow S, Sorby W, Grinnell V. Outcome of aneurysmal subarachnoid haemorrhage following the introduction of papaverine angioplasty. J Clin Neurosci 1996;3:139–142. [PubMed: 18638856]

20. Nahed BV, DiLuna ML, Morgan T, Ocal E, Hawkins AA, Ozduman K, Kahle KT, Chamberlain A, Amar AP, Gunel M. Hypertension, age, and location predict rupture of small intracranial aneurysms. Neurosurgery 2005;57:676–683. [PubMed: 16239879]

21. Orz Y, Kobayashi S, Osawa M, Tanaka Y. Aneurysm size: A prognostic factor for rupture. Br J Neurosurg 1997;11:144–149. [PubMed: 9156002]

22. Raghavan ML, Ma B, Harbaugh RE. Quantified aneurysm shape and rupture risk. J Neurosurg 2005;102:355–362. [PubMed: 15739566]

23. Rinkel GJ, Djibuti M, Algra A, van Gijn J. Prevalence and risk of rupture of intracranial aneurysms: A systematic review. Stroke 1998;29:251–256. [PubMed: 9445359]

24. Shojima M, Oshima M, Takagi K, Torii R, Hayakawa M, Katada K, Morita A, Kirino T. Magnitude and role of wall shear stress on cerebral aneurysm: Computational fluid dynamic study of 20 middle cerebral artery aneurysms. Stroke 2004;35:2500–2505. [PubMed: 15514200]

25. Ujiie H, Sato K, Onda H, Oikawa A, Kagawa M, Takakura K, Kobayashi N. Clinical analysis of incidentally discovered unruptured aneurysms. Stroke 1993;24:1850–1856. [PubMed: 8248967]

26. Ujiie H, Tachibana H, Hiramatsu O, Hazel AL, Matsumoto T, Ogasawara Y, Nakajima H, Hori T, Takakura K, Kajiya F. Effects of size and shape (aspect ratio) on the hemodynamics of saccular aneurysms: A possible index for surgical treatment of intracranial aneurysms. Neurosurgery 1999;45:119–130. [PubMed: 10414574]

27. Ujiie H, Tamano Y, Sasaki K, Hori T. Is the aspect ratio a reliable index for predicting the rupture of a saccular aneurysm? Neurosurgery 2001;48:495–503. [PubMed: 11270538]

28. Weir, B. Aneurysms Affecting the Nervous System. Baltimore, Williams & Wilkins; 1987. p. 308-363.

29. Weir B, Amidei C, Kongable G, Findlay JM, Kassell NF, Kelly J, Dai L, Karrison TG. The aspect ratio (dome/neck) of ruptured and unruptured aneurysms. J Neurosurg 2003;99:447–451. [PubMed: 12959428]

30. Weir B, Disney L, Karrison T. Sizes of ruptured and unruptured aneurysms in relation to their sites and the ages of patients. J Neurosurg 2002;96:64–70. [PubMed: 11794606]

31. Wiebers DO, Whisnant JP, Huston J 3rd, Meissner I, Brown RD Jr, Piepgras DG, Forbes GS, Thielen K, Nichols D, O'Fallon WM, Peacock J, Jaeger L, Kassell NF, Kongable-Beckman GL, Torner JC. Unruptured intracranial aneurysms: Natural history, clinical outcome, and risks of surgical and endovascular treatment. Lancet 2003;362:103–110. [PubMed: 12867109]

32. Wills S, Ronkainen A, van der Voet M, Kuivaniemi H, Helin K, Leinonen E, Frösen J, Niemela M, Jääskeläinen J, Hernesniemi JA, Tromp G. Familial intracranial aneurysms: An analysis of 346 multiplex Finnish families. Stroke 2003;34:1370–1374. [PubMed: 12750547]

33. Zweig MH, Campbell G. Receiver-operating characteristic (ROC) plots: A fundamental evaluation tool in clinical medicine. Clin Chem 1993;39:561–577. [PubMed: 8472349]
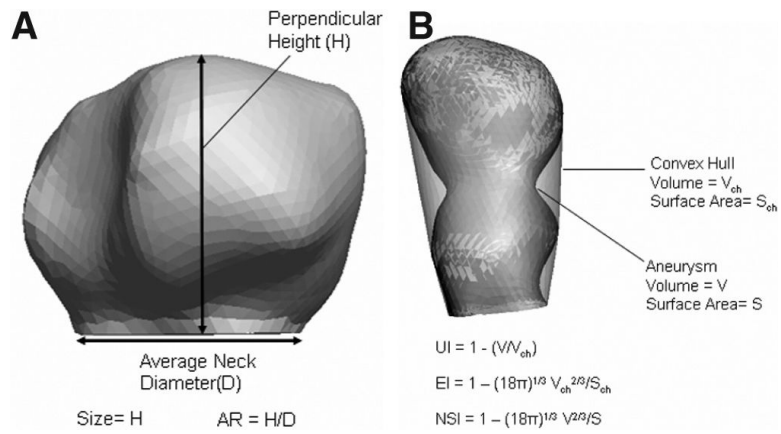
FIGURE 1.
A, definition of aspect ratio (AR). B, definition of convex hull. UI, undulation index; EI, ellipticity index; NSI, nonsphericity index.
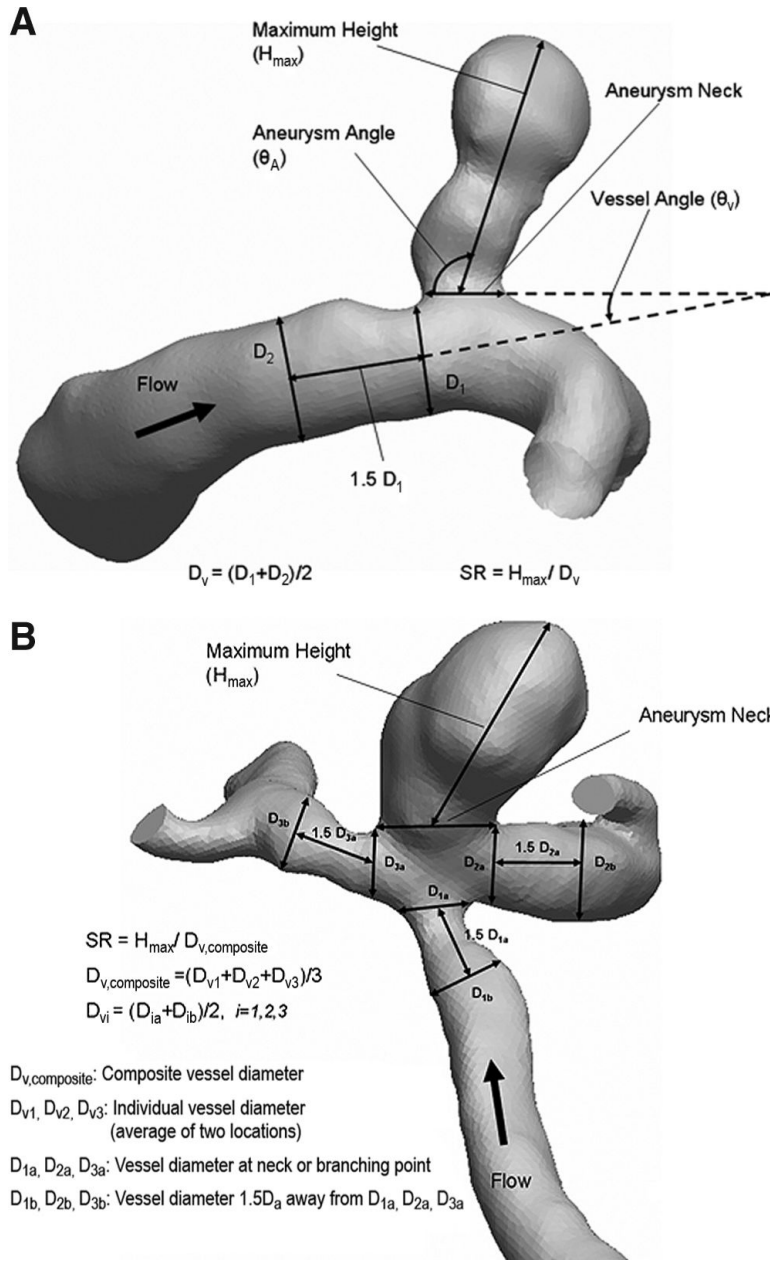
FIGURE 2.
Definition of aneurysm angle (θ_A) and vessel inlet angle (θ_V) in the viewing plane, and definition of size ratio (SR) for sidewall intracranial aneurysm (IA) (A) and terminal IA (B).
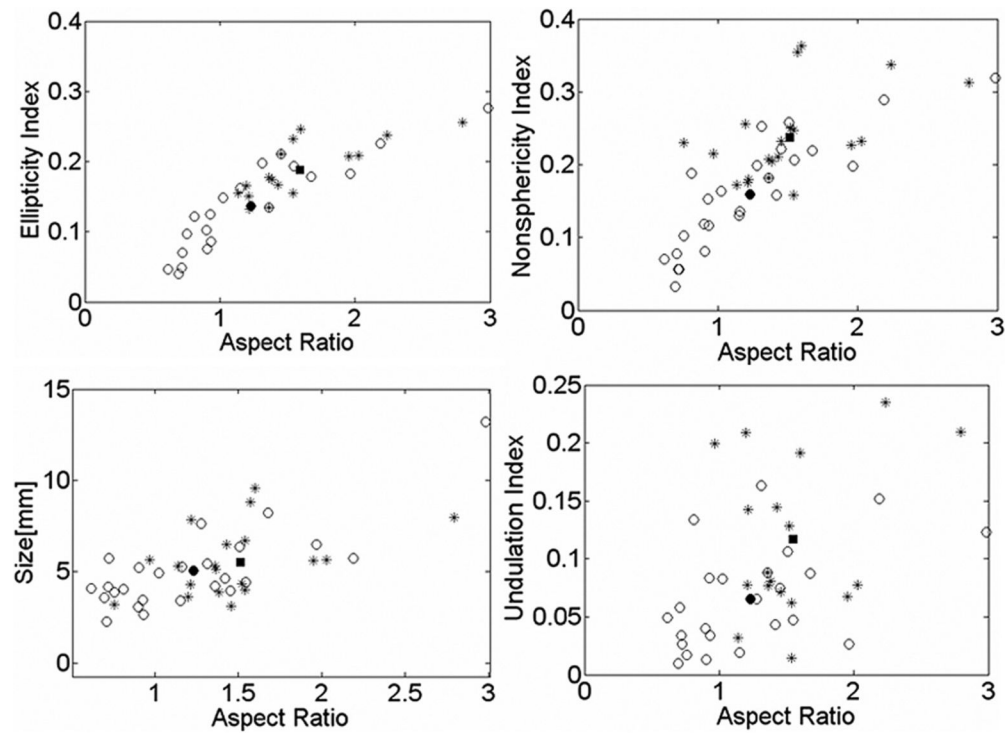
FIGURE 3.
Scatterplots for the traditional parameters. *, data points for ruptured aneurysms; ○, data points for unruptured aneurysms; ■, mean value for ruptured aneurysms; ●, mean value for unruptured aneurysms.
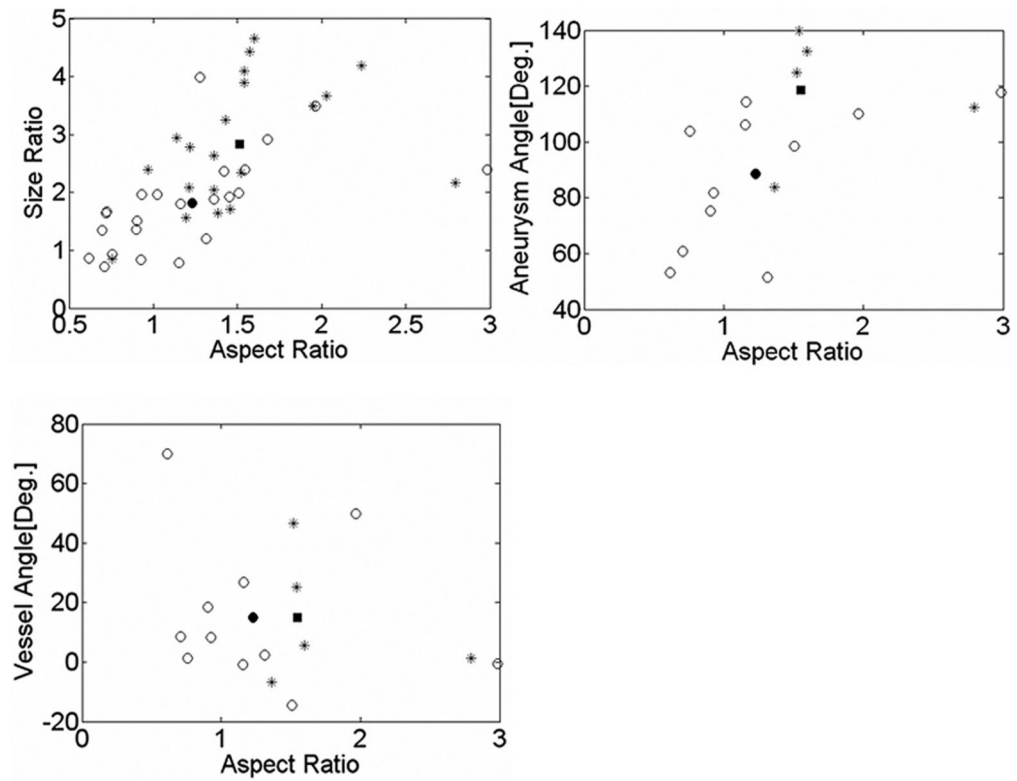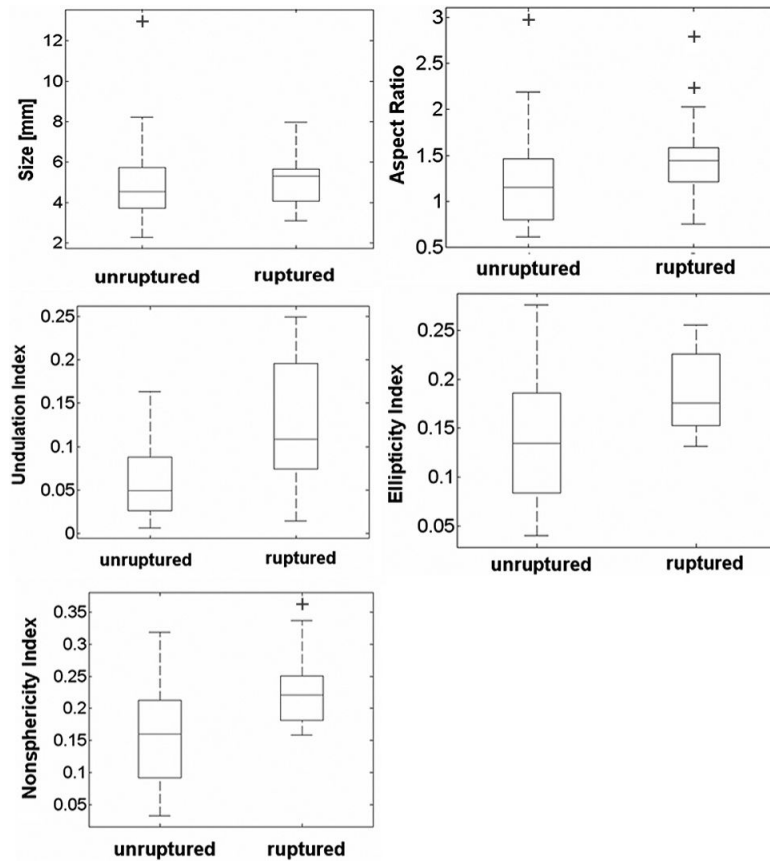
FIGURE 4.
Scatterplots for the new variables defined in this study. *, data points for ruptured aneurysms; ○, data points for unruptured aneurysms; ■, mean value for ruptured aneurysms; ●, mean value for unruptured aneurysms.

FIGURE 5.
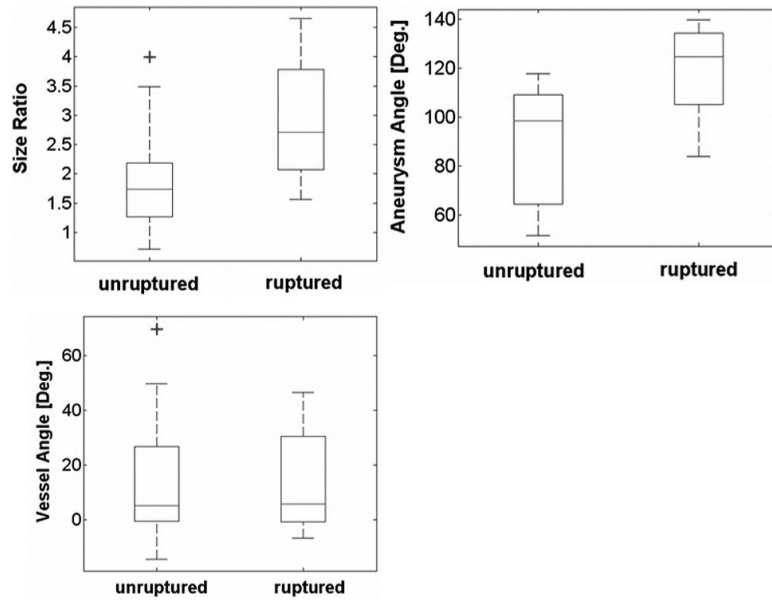Box plots for the traditional parameters. +, outlier.

FIGURE 6.
Box plots for the new parameters defined in this study. +, outlier.
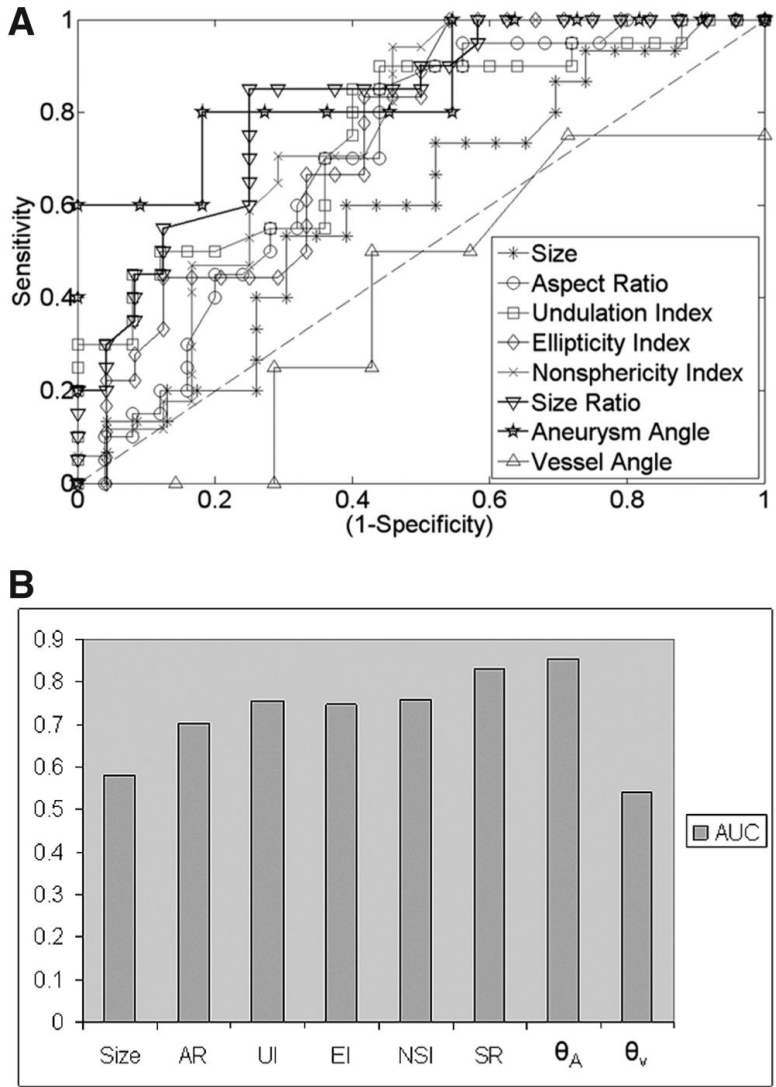
FIGURE 7.
A, receiver operating characteristic curves for all parameters. A larger area under the curve (AUC) implies higher sensitivity and higher specificity for that parameter to discriminate the two subgroups (ruptured and unruptured). Dashed line, null predictor. B, AUC values of each parameter.
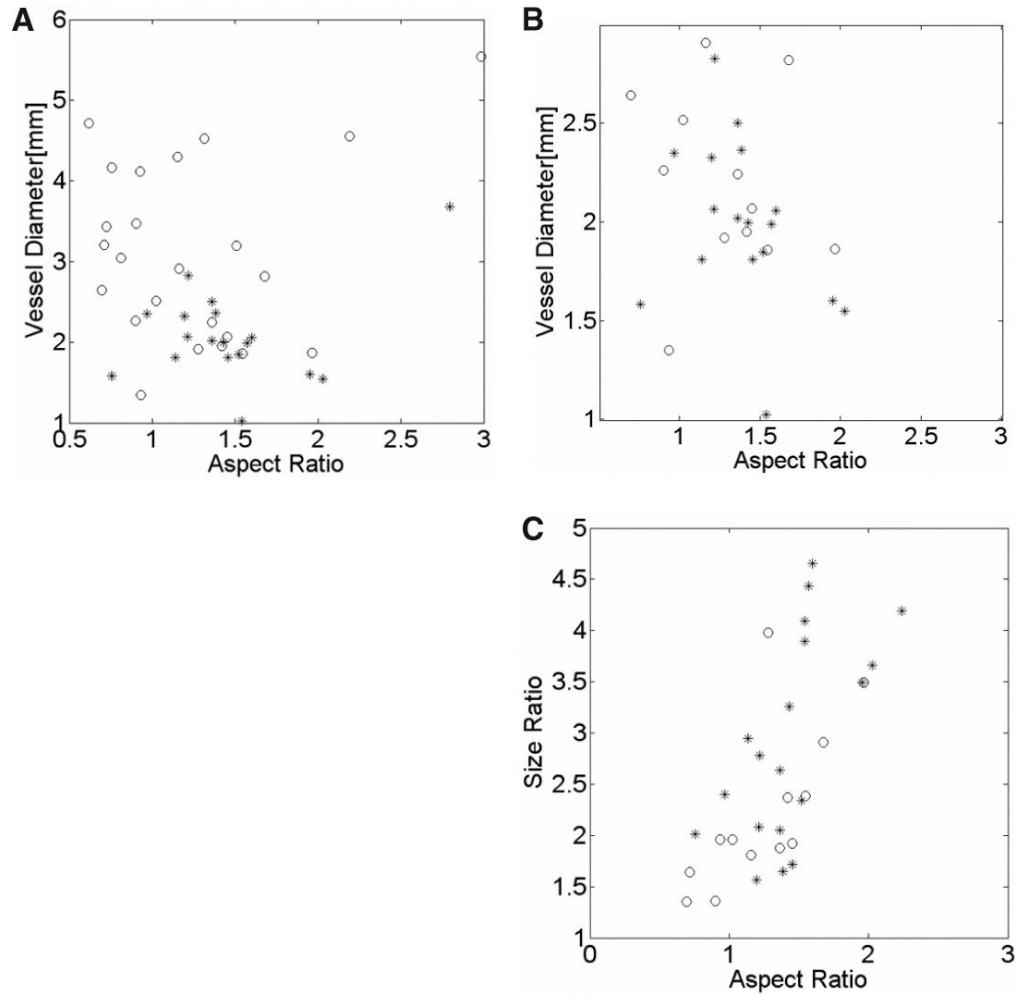
FIGURE 8.
A, vessel diameter versus aspect ratio (AR) for all aneurysms. B, vessel diameter versus AR, excluding intracranial aneurysms (IA) located on the internal carotid artery (ICA) (ophthalmic or petrous-cavernous segment of ICA). C, size ratio versus AR, excluding IAs located on the ICA (ophthalmic or petrous-cavernous segment of ICA).
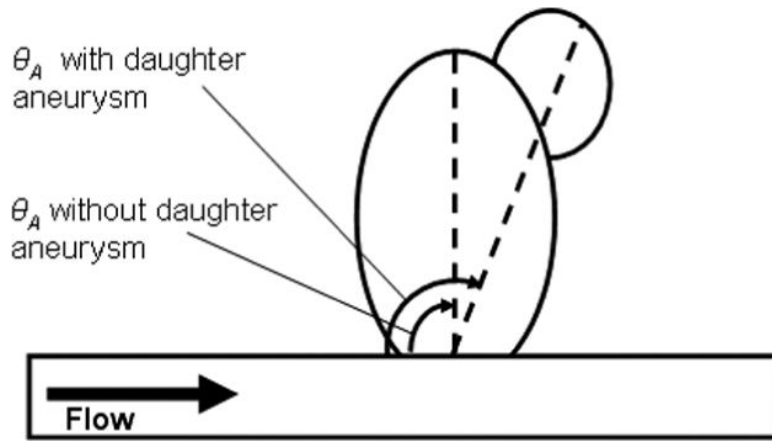
FIGURE 9.
Difference of aneurysm angle (θ_A) if a daughter aneurysm (or increased growth in the direction of the flow) is present.
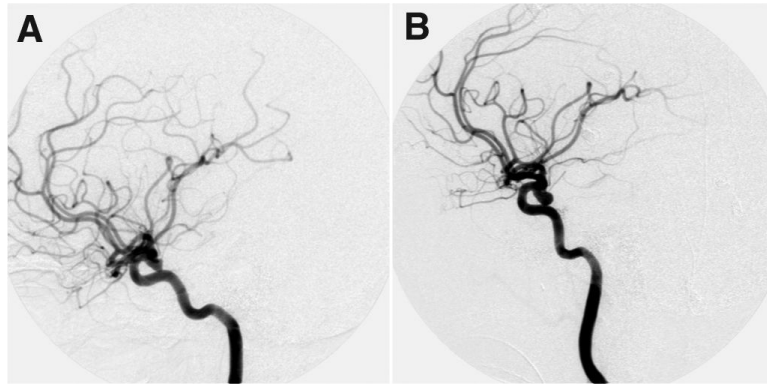
FIGURE 10.
Angiograms showing a posterior communicating artery aneurysm that was imaged 4 months before subarachnoid hemorrhage (SAH) (A) and immediately after SAH (B). The aneurysm height and vessel size remain unchanged (yielding SR, 2.6).

TABLE 1

Results from the statistical analysis for all parameters[a]

Index	Ruptured mean	Unruptured mean	P value	95% confidence limits	AUC	Optimal thresholds
Size	5.5 ± 1.9	5.1 ± 2.3	0.463	−0.622, 1.35	0.58	5.37[b]
AR	1.5 ± 0.45	1.2 ± 0.55	0.044	0.07, 0.484	0.703	1.2
UI	0.12 ± 0.07	0.063 ± 0.045	0.0009	0.0266, 0.0963	0.755	0.064
EI	0.19 ± 0.043	0.14 ± 0.062	0.003	0.0185, 0.0846	0.746	0.15
NSI	0.24 ± 0.06	0.16 ± 0.076	0.0029	0.0233, 0.106	0.757	0.17
SR	2.8 ± 1.1	1.8 ± 0.84	0.00026	0.545, 1.65	0.83	2.05
θ_A	118 ± 21	88 ± 24	0.0365	2.18, 58.1	0.854	111.5
θ_V	15 ± 26	15 ± 26	0.939	−28.7, 26.7	0.54	49.2[b]

[a] AUC, area under the curve; AR, aspect ratio; UI, undulation index; EI, ellipticity index; NSI, nonsphericity index; SR, aneurysm-to-vessel size ratio; θ_A aneurysm inclination angle; θ_V vessel angle.

[b] Not significant.

TABLE 2

Results from the multivariate logistic regression analysis for all intracranial aneurysms[a]

Step and indices	β	*P* value	Odds ratio	95% confidence interval
1				
AR	−0.402	0.1	0.669	0.414−1.08
UI	0.528	0.141	1.7	0.840−3.42
EI	0.888	0.201	2.43	0.624−9.46
NSI	−0.493	0.555	0.611	0.119−3.13
SR	0.428	0.04	1.53	1.02−2.31
2				
AR	−0.382	0.108	0.683	0.428−1.09
UI	0.354	0.067	1.43	0.976−2.08
EI	0.547	0.378	1.73	0.824−3.63
SR	0.392	0.047	1.48	1.01−2.18
3				
AR	−0.105	0.457	0.9	0.682−1.19
UI	0.456	0.014	1.58	1.1−2.27
SR	0.414	0.03	1.51	1.04−2.2
4				
UI	0.412	0.016	1.51	1.08−2.11
SR	0.342	0.032	1.41	1.03−1.92

[a] AR, aspect ratio; UI, undulation index; EI, ellipticity index; NSI, nonsphericity index; SR, aneurysm-to-vessel size ratio.

TABLE 3

Comparison of the vessel diameters in our patient group with typical diameters[a]

Location	Typical diameter[b](mm)	Unruptured (mm)	Ruptured (mm)
ICA (ophthalmic or Pet-Cav)	3.8−4.6	4.55	
ICA	3.8−4.6	3.45	3.69
AComA	0.5−3.7 (average, 2)	2.46	1.84
MCA bifurcation (mean of the 3 branches)	1.25−2.5	1.98	2.8
PComA	1.3		1.95
ACA	2.6		2.6
PCA	2.6		2.36

[a]ICA, internal carotid artery; Pet-Cav, petrous cavernous segment; AComA, anterior communicating artery; MCA, middle cerebral artery; PComA, posterior communicating artery; ACA, anterior cerebral artery; PCA, posterior cerebral artery.

[b]From, Weir B: *Aneurysms Affecting the Nervous System.* Baltimore, Williams & Wilkins, 1987, pp 308−363 (28).